ELSEVIER

Journal of Nuclear Materials 245 (1997) 147–151

journal of nuclear materials

# A method for the quantitative phase analysis of $ZrO_2$ films grown on Zr–2.5% Nb pressure tubes

M.G. Glavicic [a,*], J.A. Szpunar [a], Y.P. Lin [b]

[a] *Department of Metallurgical Engineering, McGill University, 3450 University, FDA Building, Montreal, Que., Canada H3A 2A7*
[b] *Ontario Hydro Technologies, Toronto, Ont., Canada*

Received 12 November 1996; accepted 12 February 1997

**Abstract**

A method for the quantitative phase analysis of textured corrosion formed $ZrO_2$ films on zirconium alloys using pole figure data has been developed. This method was then used to examine changes in the volume fraction of the tetragonal and monoclinic phases of $ZrO_2$ films grown on Zr–2.5% Nb as a function of heat treatments, oxide thickness and oxidizing environments.

## 1. Introduction

A major difficulty encountered during quantitative X-ray phase analysis is the existence of texture. In the past, during the examination of textured oxides grown on zirconium alloys, the texture of the two phases present has been assumed to be the same [1–3] so that X-ray diffraction techniques developed for the $ZrO_2$ system [4–7] could be applied. Conventional X-ray diffraction techniques [4] used to determine the relative amounts of the various phases require a calibration curve to be obtained from a series of samples whose relative quantities of each phase are known in advance. These methods are destructive and cumbersome in that the technique requires the materials be ground and mounted in a particular fashion which is assumed to be texture free. In the study of textured zirconium oxide films, grown on zirconium alloy coupons, these methods are of limited use in that they would require the oxide to be completely removed from its substrate and gathered in sufficient quantities so that a texture free powder sample could be fashioned. The abundance of the metastable tetragonal phase in these oxides has in the past been attributed to the effects of crystallite size, alloying impurity elements and the presence of stabilizing compressive stresses built up during oxide growth. The removal of the oxide from its substrate would relieve the compressive stresses present in the sample and possibly change the relative abundance of the tetragonal phase present since it could then transform to the room temperature and pressure stable monoclinic $ZrO_2$ phase.

When a sample is textured, the accuracy of the phase analysis technique [8] employed is dependant upon the type and sharpness of the samples texture. If the texture of the specimen is favorable, a number of clearly separated diffraction peaks from both phases will be discernible in a simple XRD scan. In this technique [8], the overall intensity and number of diffraction peaks available are then used to calculate texture parameters which can be used to calculate the volume fractions of the two phases present. A shortcoming of this technique for the $ZrO_2$ system is that its accuracy is dependant upon the number of diffraction peaks discernible. As is the case in many oxides, the positions of the diffraction peaks of the zirconium oxide polymorphs are close and in some cases overlap. In addition for thin $ZrO_2$ films, diffraction peaks from the substrate further restrict the number of diffraction peaks available for phase analysis, making this technique questionable. Another technique [9] involving the use of specialized equipment has also been proposed. In this procedure [9], an X-ray powder diffractometer in combination with a specially designed computer controlled specimen holder is used to tilt and rotate the sample during a $\theta$ versus $2\theta$ scan. The tilting and rotation of the sample scans the

* Corresponding author.


*PII* S0022-3115(97)00017-2

scattering vector of the diffraction peak being examined to within 60° of the sample normal. This technique allows the texture of the specimen to be taken into account provided the samples poles lie entirely within the region scanned.

The technique proposed in this paper determines the relative volume fractions in multiphase textured materials from pole figure data. This technique is truly non-destructive in that it does not require the sample being examined to be removed from its substrate and ground in order to negate any texturing effects, nor does it require a calibration curve to be determined for the particular material being examined.

## 2. Theory

For an untextured polycrystalline multiphased powder specimen, the observed intensity of a diffraction peak in a XRD scan can be described by the following expression [10]:

$$I(hkl) = K \times G(hkl) \times V, \tag{1}$$

where $K$ is a constant of the apparatus and radiation used, and $V$ is the volume fraction of the phase being examined. $G(hkl)$ is given by

$$G(hkl) = \left( \frac{|F|^2 p e^{-2M}}{v^2} \right) \left( \frac{1 + \cos^2 2\theta_B}{\sin^2 \theta_B \cos \theta_B} \right), \tag{2}$$

where $F$ is the structure factor, $v$ is the volume of the crystallographic unit cell, $e^{-2M}$ is the temperature factor (a function of $\theta_B$), $p$ is the multiplicity of the crystallographic plane being examined and the remaining term is the Lorentz polarization factor.

Under normal conditions, when a $\theta$ versus $2\theta$ scan is performed on a specimen in reflection mode, the various diffraction peaks observed originate from crystallographic planes that satisfy the Bragg equation. In this geometry, for a particular diffraction peak, the scattering vector $S(hkl)$ is the perpendicular bisector between incoming and reflected X-rays. By definition the scattering vector $S(hkl)$, is a vector which is perpendicular to the crystallographic plane defined by the Miller indices $h$, $k$ and $l$. Therefore, a typical XRD scan is a sampling of the number crystallographic planes parallel to the specimens surface. In order to account for a preferred orientation or texture in the polycrystalline specimen being examined, a pole figure can be measured. In this procedure, a particular diffraction peak is selected from the diffraction pattern obtained for the specimen. The Bragg angle $\theta_B$, of the incoming radiation and detector angle $2\theta_B$, are then selected to center on the peak selected. The specimen is then tilted and rotated to scan the scattering vector $S(hkl)$ within the specimens reference frame which in effect samples the orientational distribution of the crystals in the polycrystalline sample. Typically the receiving slits in front of the detector are selected with a 0.6° acceptance angle so that shifts in the position of the diffraction peak during sample tilting and rotation due to stress fields present in the specimen can be taken into account.

During the measurement of a pole figure, three other factors must also be taken into account for the proper normalization and correction of the individual pole figures: absorption, defocussing and background corrections. The absorption of the X-rays by the oxide layer is a function of its thickness $t$, linear absorption coefficient $\mu$, the Bragg angle $\theta_B$ and the angle $\alpha$ between the scattering vector and the sample normal. For pole figures that are measured in the standard Schultz reflection geometry the correction factor $f_{abs}$ has the functional form

$$f_{abs}(\mu, t, \alpha, \theta_B) = \frac{1 - e^{-2\mu t / \sin \theta_B}}{1 - e^{-2\mu t/(\cos \alpha \sin \theta_B)}}. \tag{3}$$

Changes in observed intensities due to defocussing $D(\alpha)$ of the incident X-ray beam upon the specimen surface are determined by the running of a 'random' untextured sample under the same conditions which the actual specimen is to be measured. The 'random' samples are prepared from chemically pure powders and are checked for any preferred orientation. Background counting rates in the specimen $B_s(\alpha)$ and the 'random' sample $B_r(\alpha)$ are then used so that each intensity measured $I_m(\alpha, \beta)$ becomes a corrected intensity $I_c(\alpha, \beta)$ where

$$I_c(\alpha, \beta) = \left[ I_m(\alpha, \beta) - B_s(\alpha = 0) \frac{B_r(\alpha)}{B_r(\alpha = 0)} \right] \times f_{abs} \frac{D(\alpha = 0)}{D(\alpha)}. \tag{4}$$

The pole figures are then integrated numerically, with each data point in the pole figure accorded a weight that is proportional to the fraction of the powder diffraction cone being sampled:

$$I_t(hkl) = \sum_{\alpha} \sum_{\beta} I_c(\alpha, \beta) \sin(\alpha) \Delta\alpha \Delta\beta. \tag{5}$$

The total integrated intensities $I_t(hkl)$ of the $(11\bar{1})_m$, $(111)_m$ monoclinic and $(111)_t$ tetragonal pole figures are then used to construct an integrated intensity ratio $X_m$

$$X_m = \frac{I_t(11\bar{1})_m + I_t(111)_m}{I_t(11\bar{1})_m + I(111)_m + I_t(111)_t} \tag{6}$$

which is commonly used in the phase analysis of the $ZrO_2$ system [4,6,7,9]. With the aid of Eq. (1), a formula for the volume fraction of the monoclinic phase $V_m$ can be obtained:

$$V_m = \frac{PX_m}{1 + (P - 1)X_m}, \tag{7}$$

where $P$ is given by

$$P = \frac{G(111)_t}{G(11\bar{1})_m + G(111)_m}. \tag{8}$$

For Cu $K_\alpha$ radiation, the calculated value for $P$ becomes 1.381 [9].

## 3. Sample preparation

The samples for this study were all cut from as received Zr–2.5% Nb pressure tubes. In the first stage of preparation, portions of the tubes were placed in a furnace so that these portions could undergo heat treatment processes of 100 h at 400°C and 6 h at 500°C. The purpose of these treatments was to change the phase composition of the alloy from its as received β-Zr phase to the (ω + β)-Zr and β-Nb phases, respectively. Coupons ($10 \times 25$ mm$^2$) were then cut such that the radial direction of the tube corresponded to the normal direction of the sample surface. All samples were then polished mechanically down to a 600 grit paper finish, followed by polishing with 9 μm diamond paste to remove the 600 grit scratches. Ammonium dichromate powder with a 0.5% HF solution was then used to give the samples a mirror-like finish.

A portion of these samples, which had not undergone a heat treatment, were then given a brief polish with 1 μm diamond paste and then placed in an autoclave filled with steam and maintained at a temperature of 673 K for periods of 168, 48, 10 and 1.5 h. The remainder of the samples in the heat-treated or as received condition were then placed in a steam filled autoclave for a period of 24 or 350 h, where upon they were placed in a solution of LiOH (pH = 10.5) at a temperature of 583 K for a period of 56 days. At each stage of the oxidation process employed, the samples were visually inspected for signs of spalling. The thickness of the oxide films obtained for both sets of samples were then determined by Fourier transform infrared interferometry (FTIR) using the procedure developed by Ramasubramanian et al. [14], for zirconium alloy corrosion films. The pole figures, in the form of a 5° grid measurement pattern, were then obtained with a Siemens D-500 texture goniometer equipped with a copper target.

## 4. Results and discussion

Using the procedure described in this paper, the evolution of the tetragonal phase as a function of oxide thickness and oxidation time was examined for samples exposed to a 673 K steam environment for various periods of time. Fig. 1 shows the evolution of the computed volume fraction of the tetragonal phase and oxide thickness as a function of time spent in a 673 K steam environment. The thickness of the oxide obtained for the 7 day steam exposure (4.1 μm) was somewhat higher than what would be expected for Zr–2.5% Nb pressure tubes under the exposed conditions. An oxide thickness of 2.5–3 μm thick would be expected under these conditions and it is suspected that surface preparation may have contributed to an

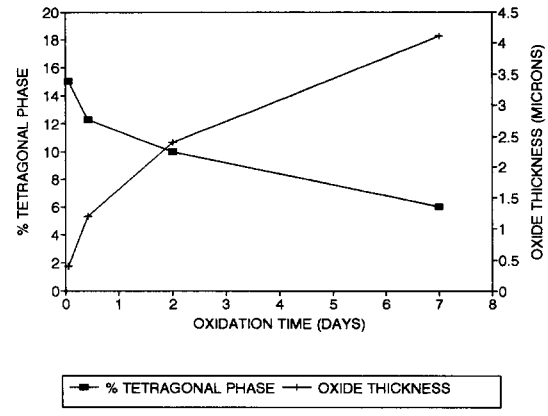


Fig. 1. Computed volume fraction of the tetragonal phase for 673 K steam-oxidized samples.

increased oxide thickness. The computed volume fraction of the tetragonal phase with time clearly decreases quite rapidly as the thickness of the oxide increases. These results are consistent with those reported in the past using X-Ray diffraction techniques [1,3,11] and Raman spectroscopy [11]. Barberis [1] modelled the evolution of the tetragonal phase in terms of a Johnson Mehl Avrami (JMA) annealing effect in zircalloy-4 samples. In this model, a thin oxide layer is formed at time '$t$' at the metal/oxide interface, whose volume fraction of the tetragonal phase is approximately 35%. As time elapses the tetragonal phase within the layer transforms to the stable monoclinic phase according to a JMA law. Concurrently, while this transformation occurs, other new layers of oxide are being formed at the new metal/oxide interface which will also transform in the same manner. A similar explanation of results was proposed by Godlewski et al. [11] with the aid of by X-ray diffractometer and Raman spectroscopy techniques. In their explanation, based upon a series of Raman spectroscopy measurements on tapered sections polished at angles between 2 and 5°, a thin layer of oxide is formed at the metal/oxide interface, which has a relative tetragonal volume fraction of 40%. Adjacent to this layer are two other layers of different thicknesses with 15% and 3% tetragonal contents. The high volume fractions of the tetragonal phase in layers adjacent to the metal/oxide interface predicted by these studies in comparison to those presented here can be attributed to the possible effects of oxide texture and compositional differences in the specimens examined. Lin et al. [12] have shown that texture can affect the relative intensities of the Raman oxide peaks observed, in that they change with sample orientation and incident angle of the incoming polarized laser beam. Pole figures, Fig. 2, measured for oxides grown on Zr–2.5% Nb coupons show that conventional XRD techniques may overestimate the volume fractions of the tetragonal $ZrO_2$ layer adjacent to the metal/oxide interface as computed from the fitting of data

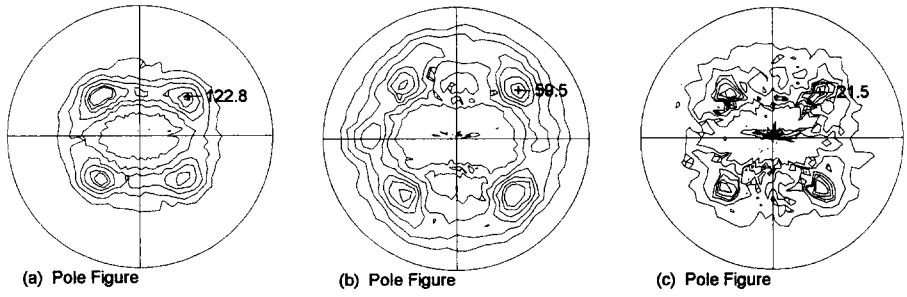


Fig. 2. Unnormalized pole figures of monoclinic and tetragonal phases: (a) $(11\bar{1})_m$, (b) $(111)_m$, (c) $(111)_t$.

with the JMA law due to the existence of texture in the tetragonal phase of the oxide. Fig. 2 shows the unnormalized pole figures for the $(11\bar{1})$ and (111) planes of the monoclinic phase, and the (111) planes of the tetragonal phase for an oxide grown in steam for a period of 10 h.

The center of each pole figure is the region which would be measured with conventional XRD techniques. Clearly a weak pole exists at the center of the tetragonal pole figure, which would result in an overestimation of the tetragonal volume fraction being computed using conventional XRD techniques that do not take the texture of the oxide into account. In the past, in order to justify the use of conventional XRD powder techniques on these highly textured oxides, it has been assumed that the textures of the two phases present are the same and that the textures of the two phases do not affect the tetragonal volume fractions being computed. In the procedure outlined in this paper, no assumptions have been made and the texture of the phases present does not have to be the same in order for the procedure to work. In addition to texture effects, compositional differences in the alloys also cannot be discounted. For example, Barberis [1] demonstrated that an increased Sn content in the alloys examined lowered the volume fraction of the tetragonal phase.

Effects in the calculated volume fraction due to sample mounting and statistical fluctuations in counting rates were investigated by the running of a single sample four times consecutively (10 h steam sample). After each run the sample was removed and remounted. The values calculated for each of the four trial runs are tabulated in Table 1.

Analysis of these values shows that the maximum deviation from the mean value computed is 0.43%. This indicates that the fluctuations in tetragonal content observed in Fig. 1 are real and can be observed using the described method.

The samples that were oxidized in steam followed by an aqueous environment for a period of 56 days displayed remarkable different volume fractions of the tetragonal phase from what would be expected from samples that were oxidized in steam only (see Fig. 1). The computed values for each specific sample are shown in Table 2. The first remarkable feature is that the tetragonal phase content for the first two samples in Table 2 are about the same even though the oxides are of different thicknesses. Based upon the trend shown in Fig. 1, one would expect the tetragonal content to be somewhat higher in the first sample, which has a thinner oxide layer. This discrepancy in tetragonal content from what would be expected from the first two oxides of different thicknesses shown in Table 2 may be explained in terms of the availability of hydrogen in the aqueous solution which is known to facilitate the transformation of the tetragonal phase to the monoclinic phase [13]. The next feature of interest is that the application of a heat treatment increases the sample corrosion resistance and as a result, decreases the overall thickness of the oxide film grown on samples that were placed in the steam-filled autoclave for 350 h. This result is consistent with other studies where improved corrosion resistance was obtained by the application of heat treatments [15].

In addition, a comparison of the computed volume fractions for specimens that had undergone the same heat treatment process showed that the tetragonal content calculated for oxides grown for 24 h in steam did not vary significantly from those grown for 350 h in steam. The preliminary results shown here clearly illustrate the role that heat treatments play in governing the overall oxide thickness and how an aqueous environment may affect the volume fraction of the tetragonal phase present in an oxide of a given thickness. In future experiments, the technique described here will be used to further examine the evolu-

Table 1
Variations in computed tetragonal volume fractions for the 10 h steam sample

| | Computed tetragonal volume fraction |
|---|---|
| Trial 1 | 12.18% |
| Trial 2 | 12.15% |
| Trial 3 | 12.17% |
| Trial 4 | 12.73% |
| Maximum deviation from mean value | 0.43% |

Table 2
Computed tetragonal volume fractions of heat treated samples placed in 583 K LiOH solution for 56 days

| Heat treatment | Time spent in 673 K steam environment (h) | Oxide thickness (μm) | Computed tetragonal volume fraction ±0.43% |
|---|---|---|---|
| None | 24 | 1.67 | 7.51% |
| None | 350 | 2.26 | 7.41% |
| 100 h, 673 K | 24 | 1.71 | 6.28% |
| 100 h, 673 K | 350 | 1.79 | 5.65% |
| 6 h, 773 K | 24 | 1.45 | 6.78% |
| 6 h, 773 K | 350 | 1.42 | 6.58% |

tion of the tetragonal volume fraction as a function of heat treatment, oxidation environment and sample preparation.

## 5. Conclusion

A method to determine the volume fraction of the tetragonal and monoclinic phases in textured $ZrO_2$ films grown on Zr–2.5% Nb coupons has been developed. This method is an improvement from the techniques presently being employed for oxides grown on zirconium alloys in that it is a quantitative method that is not subject to errors due to the presence of oxide texture. The evolution of the tetragonal phase content as a function of oxide thickness can be examined using this technique and the results obtained in this study were consistent with previous results.

## References

[1] P. Barberis, J. Nucl. Mater. 226 (1995) 34.
[2] C. Roy, G. David, J. Nucl. Mater. 37 (1970) 71.
[3] H.J. Beie, A. Mitwalsky, F. Garzarolli, H. Ruhmann, H.J. Sell, Zirconium in the Nuclear Industry: 10th Int. Symp., ASTM STP 1245 (1994) 615.
[4] H. Toraya, M. Yoshimura, S. Somiya, Commun. Am. Ceram. Soc. 64 (1984) C119.
[5] P. Duwez, F. Odell, J. Am. Ceram. Soc. 32 (1949) 180.
[6] R.C. Garvie, P.S. Nicholson, J. Am. Ceram. Soc. 55 (1972) 303.
[7] E.D. Whitney, Trans. Faraday Soc. 61 (1965) 1991.
[8] M.J. Dickson, J. Appl. Crystallogr. 2 (1969) 176.
[9] R. Fillit, P. Homerin, J. Schafer, H. Bruyas, F. Thevenot, J. Mater. Sci. 22 (1987) 3566.
[10] D.L. Porter, A.H. Heuer, J. Am. Ceram. Soc. 62 (1979) 298.
[11] J. Godlewski, J.P. Gross, M. Lambertin, J.F. Wadier, H. Weidinger, ASTM-STP 1132 (1991) 416.
[12] Y.P. Lin, O.T. Woo, D.J. Lockwood, Mater. Res. Soc. Symp. Proc. Vol. 343 (1994) 487.
[13] F. Garzarolli, H. Seidel, R. Tricot, J.P. Gross, Zirconium in the Nuclear Industry: 9th Int. Symp., ASTM STP 1132 (1991) 395.
[14] N. Ramasubramanian, V.C. Ling, M.H. Schankula, R.J. Chenier, in: Post-Irradiation Examination Techniques for Water Reactor Fuel, IAEA, IWGFPT 37, Vienna, 1991, p. 124.
[15] V.F. Urbanic, R.W. Gilbert, in: Fundamental Aspects of Corrosion on Zirconium Base Alloys in Water Reactor Environments, IAEA, IWGFPT, Vienna, 1990, p. 262.